Eur. Phys. J. E (2015) **38**: 42
DOI 10.1140/epje/i2015-15042-3

THE EUROPEAN PHYSICAL JOURNAL E

Regular Article

# Three-sphere low-Reynolds-number swimmer with a passive elastic arm

Alessandro Montino[1] and Antonio DeSimone[1,2,a]

[1] GSSI - Gran Sasso Science Institute, viale Francesco Crispi 7, 67100 L'Aquila, Italy
[2] SISSA - International School for Advanced Studies, via Bonomea 265, 34136 Trieste, Italy

Received 24 September 2014 and Received in final form 29 January 2015
Published online: 22 May 2015


**Abstract.** One of the simplest model swimmers at low Reynolds number is the three-sphere swimmer by Najafi and Golestanian. It consists of three spheres connected by two rods which change their lengths periodically in non-reciprocal fashion. Here we investigate a variant of this model in which one rod is periodically actuated while the other is replaced by an elastic spring. We show that the competition between the elastic restoring force and the hydrodynamic drag produces a delay in the response of the passive elastic arm with respect to the active one. This leads to non-reciprocal shape changes and self-propulsion. After formulating the equations of motion, we study their solutions qualitatively and numerically. The leading-order term of the solution is computed analytically. We then address questions of optimization with respect to both actuation frequency and swimmer's geometry. Our results can provide valuable conceptual guidance in the engineering of robotic microswimmers.

## 1 Introduction

In his celebrated 1977 lecture [1], Purcell formulated the famous *scallop theorem*. According to this result, in order to achieve self-propulsion at low Reynolds number, a swimmer must change its shape in a way that is not invariant under time-reversal (see also [2] for a recent review and [3, 4] for a non-trivial example in the context of biological locomotion). Thus, a micron-sized scallop trying to swim through the reciprocal opening and closing of its valves would achieve no net motion. Two of the simplest model swimmers that are able to beat the scallop theorem are Purcell's three-link swimmer [1] and the three-sphere swimmer by Najafi and Golestanian [5]. These two model swimmers, which have already been studied in great detail (see *e.g.* [6–15] and the many references cited therein), rely on the same idea: in order to break time-reversal symmetry, two shape parameters are needed. The two shape parameters change periodically in time, so the swimmer's shape evolves by tracing a loop in shape space. Locomotion is possible only if the loops are non-trivial (namely, if they enclose a portion of the plane with positive area). In their 2012 paper [16], Passov and Or studied a variant of Purcell's three-link swimmer in which the front joint angle is periodically actuated while the evolution of the rear joint is governed by a passive torsional spring. In this work, we pursue a similar idea and study what happens if the rear rod of the three-sphere swimmer is replaced by an elastic spring. The problem we obtain is simpler than the one treated in [16] because, unlike the three-link swimmer, the three-sphere swimmer does not have rotational degrees of freedom. The simpler structure of the three-sphere swimmer provides us with a very vivid representation of how non-trivial loops in the shape space are formed thanks to the competition between elastic restoring force and hydrodynamic viscous drag. This simple principle may find wide applicability in the study of biological microscopic swimmers, and in the design of artificial ones.

The rest of this paper is organised as follows. In sect. 2 we describe the model and formulate the equations of motion. A qualitative study of the system that governs the dynamics of the passive arm is presented in sect. 3.1, while numerical solutions are discussed in sect. 3.2. In sect. 4 we derive leading-order expressions of the swimmer's velocity, displacement and expended power through a small-amplitude asymptotic expansion. In sect. 5 we study several optimal swimming problems by considering both *stroke* optimization (optimal actuation frequency, with respect to several alternative choices of the performance measure) and *shape* optimization (length of the elastic arm). This detailed analysis of a simple model can provide useful conceptual guidance in the engineering of more complex robotic microswimmers.

[a] e-mail: desimone@sissa.it

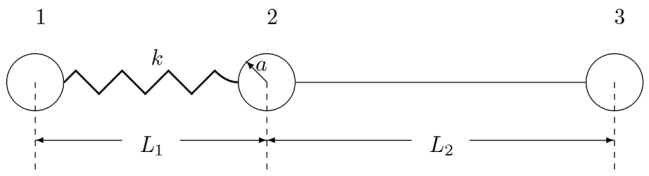


**Fig. 1.** The three-sphere swimmer with a passive elastic arm. It is very similar to the three-sphere swimmer by Najafi and Golestanian [5], with the difference that one of the two arms has been replaced by an elastic spring.

## 2 Problem formulation

Consider a swimmer composed of three spheres of radius $a$ linked by two arms. Suppose that a periodic shape change of the swimmer is assigned by two functions $L_1(t)$, $L_2(t)$ with period $T$. Then $t \mapsto (L_1(t), L_2(t))$ is a closed curve in the shape space $(L_1, L_2)$. To leading order in the amplitude of the length change, the net displacement of the swimmer in one period is proportional to the area enclosed by this curve, see [5, 17]. Further details can be found in [11–15].

We consider a variation of the three-sphere swimmer in which the rear rod is replaced by an elastic spring with elastic constant $k$ as in fig. 1. Our swimmer is able to control the length of the front rod with a prescribed periodic function $L_2(t)$, while the evolution of $L_1$ is governed by the balance of elastic and hydrodynamic (viscous) forces. Let us denote with $\mu$ the fluid viscosity, with $f_i$ the force exerted by the $i$-th sphere on the fluid and with $v_i$ the velocity of the $i$-th sphere. Following [5, 17], we use the Oseen tensor and the approximation $\frac{a}{L_i} \ll 1$ to obtain the following linear relation between hydrodynamic forces and velocities:

$$v_1 = \frac{f_1}{6\pi\mu a} + \frac{f_2}{4\pi\mu L_1} + \frac{f_3}{4\pi\mu(L_1+L_2)}, \tag{1}$$

$$v_2 = \frac{f_1}{4\pi\mu L_1} + \frac{f_2}{6\pi\mu a} + \frac{f_3}{4\pi\mu L_2}, \tag{2}$$

$$v_3 = \frac{f_1}{4\pi\mu(L_1+L_2)} + \frac{f_2}{4\pi\mu L_2} + \frac{f_3}{6\pi\mu a}. \tag{3}$$

We want the swimmer to be able to move without the help of external forces, and we neglect the inertial forces due to the sphere masses, consistently with the low-Reynolds-number regime we are studying. This implies that the following condition (global force balance) must hold:

$$f_1 + f_2 + f_3 = 0. \tag{4}$$

Moreover, the geometry of the system implies the following kinematic relations:

$$\dot{L}_1 = v_2 - v_1, \tag{5}$$

$$\dot{L}_2 = v_3 - v_2. \tag{6}$$

Finally, as a consequence of Newton's third law of motion, the fluid exerts on the $i$-th sphere a force which is equal and opposite to $f_i$. Since the forces acting on sphere 1 are the elastic force and the viscous drag exerted by the fluid, the force balance equation for sphere 1 is

$$k(L_1 - l_1) - f_1 = 0, \tag{7}$$

where $l_1$ is the rest length of the spring. We assume that the swimmer is able to control the time evolution of $L_2$ so that $L_2$ and $\dot{L}_2$ are known functions of time. If we think of eqs. (1)–(7) as seven equations in the unknowns $f_1$, $f_2$, $f_3$, $v_1$, $v_2$, $v_3$, $\dot{L}_1$ we might solve the system and find $\dot{L}_1$ as a function of $L_2$, $\dot{L}_2$ and $L_1$. We obtain in this way an ODE for $L_1$.

We use eqs. (1)–(6) to express forces and velocities as functions of $L_1$, $\dot{L}_1$, $L_2$, $\dot{L}_2$. If we plug the resulting expressions into eq. (7) we get

$$\dot{L}_1 = -\frac{k}{\mu l} G(\mathbf{L})(L_1 - l_1) - F(\mathbf{L})\dot{L}_2, \tag{8}$$

where $l$ is a characteristic length measuring the size of the swimmer, $\mathbf{L} = (L_1, L_2)$, and the dimensionless coefficients are given by

$$F(\mathbf{L}) = \left(\frac{1}{2L_2} - \frac{1}{3a}\right)^{-1} \left(\frac{1}{4L_2} + \frac{1}{4L_1} - \frac{1}{4(L_1+L_2)} - \frac{1}{6a}\right),$$

$$G(\mathbf{L}) = \frac{l}{\pi}\left[\left(\frac{1}{3a} - \frac{1}{2L_1}\right) + \left(\frac{1}{4L_1} + \frac{1}{4L_2} - \frac{1}{4(L_1+L_2)} - \frac{1}{6a}\right)^2 \left(\frac{1}{2L_2} - \frac{1}{3a}\right)^{-1}\right].$$

Equation (8) is a non-autonomous ODE for $L_1$. In the following we will consider periodic harmonic deformations

$$L_2(t) = l_2(1 + \epsilon \sin(\omega t)), \tag{9}$$

where $\omega$, $\epsilon > 0$ and $\epsilon$ is small. The natural choice for the characteristic length is $l = l_1 + l_2$. Clearly, we will assign this deformation so that $L_2(t) > 2a$ for every $t$, to avoid overlapping of spheres 2 and 3. This is guaranteed if

$$\epsilon < \epsilon_{\max} := 1 - 2a/l_2. \tag{10}$$

We would like to stress the fact that $G(\mathbf{L})$ is strictly positive if $L_1, L_2 > 2a$. This is not difficult to check and will be important in some of the following arguments.

Now we would like to non-dimensionalize our equation using the following space and time variables: $\tau = \omega t$, $\alpha = a/l$, $\Lambda_i = L_i/l$, $\lambda_i = l_i/l$ $(i = 1, 2)$. If we use the new variables eq. (8) becomes

$$\Lambda_1' = -\frac{1}{\Omega}\tilde{G}(\boldsymbol{\Lambda})(\Lambda_1 - \lambda_1) - \tilde{F}(\boldsymbol{\Lambda})\Lambda_2', \tag{11}$$

where $\boldsymbol{\Lambda} = (\Lambda_1, \Lambda_2)$, $\tilde{G}(\boldsymbol{\Lambda}) = G(l\boldsymbol{\Lambda})$, $\tilde{F}(\boldsymbol{\Lambda}) = F(l\boldsymbol{\Lambda})$, the prime symbol indicates the derivative with respect to $\tau$, $\Omega$ is a dimensionless parameter defined as follows:

$$\Omega := \omega\mu l/k, \tag{12}$$

and

$$\Lambda_2(\tau) = \lambda_2(1 + \epsilon \sin(\tau)). \tag{13}$$

Notice that the parameters $\omega$, $l$, $\mu$, $k$ affect the response of the system only through the dimensionless parameter $\Omega$.

## 3 Qualitative and numerical study of the problem

The aim of this section is to gather some intuition on the behaviour of the system before turning to its detailed analysis via asymptotic expansions. We discuss some qualitative properties of solutions in sect. 3.1 and some numerical simulations in sect. 3.2. Both numerical simulations and qualitative study show that non-trivial loops in the shape space are formed, therefore the swimmer is able to achieve self-propulsion. The net displacements produced in this way, however, become vanishingly small when the parameter $\Omega$ is either too high or too low.

### 3.1 Qualitative properties of the solution

Here we use the variable $x = \Lambda_1 - \lambda_1$ to simplify the notation. Let us rewrite (11) as

$$x' = f(\tau, x), \tag{14}$$

where

$$f(\tau, x) = -\frac{1}{\Omega}\tilde{G}(\lambda_1 + x, \Lambda_2)x - \tilde{F}(\lambda_1 + x, \Lambda_2)\Lambda_2', \tag{15}$$

and $\Lambda_2(\tau)$ is given by eq. (13). We would like to study the properties of the solutions to the Cauchy problem

$$\begin{cases} x' = f(\tau, x), \\ x(0) = x_0. \end{cases} \tag{16}$$

The initial data $x_0$ with physical relevance are those such that

$$x_0 > \overline{x}_0 := 2\alpha - \lambda_1, \tag{17}$$

namely the ones corresponding to configurations in which spheres 1 and 2 do not overlap. It is not difficult to verify that if $\epsilon$ is small enough then $f(\tau, \overline{x}_0) > 0$ for every time $\tau$. This implies that the interval $[\overline{x}_0, +\infty)$ is invariant for the dynamics. Physically, this means that if spheres 1 and 2 do not overlap at time $\tau = 0$, they will not overlap at any time $\tau > 0$. The velocity field $f$ is smooth on $\mathbb{R} \times [\overline{x}_0, +\infty)$, so classical theorems guarantee local existence and uniqueness of solutions to problem (16). We also notice that if $x$ is large enough then $f(\tau, x) < 0$ for every $\tau$. This implies that the solutions are bounded, hence global in time.

By expanding $\tilde{G}$ in Taylor series with respect to the second variable we can rewrite eq. (14) as follows:

$$x' = -\frac{1}{\Omega}\tilde{G}(\lambda_1 + x, \lambda_2)x + \epsilon g(\tau, x, \epsilon), \tag{18}$$

an autonomous system with a periodic perturbation. Notice that the function $g$ depends also on $\Omega$, even if we do not make this dependence explicit in the notation. The period of the perturbation is $2\pi$. The unperturbed system

$$x' = -\frac{1}{\Omega}\tilde{G}(\lambda_1 + x, \lambda_2)x \tag{19}$$

has a unique equilibrium point at $x = 0$. This equilibrium is stable and globally asymptotically stable, as can be seen with the help of the Lyapunov function $V(x) = x^2$. So the unperturbed system admits a periodic (constant) solution. To study the perturbed system we refer to some classical results that can be found in [18], chapter 6, and that we collected in appendix A. In our case the variational system of the unperturbed equation with respect to its periodic solution, corresponding to system (A.5) in appendix A, is

$$y' = -\frac{1}{\Omega}G_0 y, \tag{20}$$

where $G_0 := G(l_1, l_2)$. Notice that $G_0 > 0$ under the natural assumption $l_1, l_2 > 2a$. The characteristic multiplier of this system is $e^{-2\pi G_0/\Omega}$. Since it is in modulus less than one, we can apply theorems A.1 and A.2. It follows from theorem A.1 that for small enough values of $\epsilon$ the perturbed system (18) admits one and only one periodic orbit. In addition, theorem A.2 can be invoked to prove that this periodic orbit is asymptotically stable for small $\epsilon$. We claim that a stronger property holds: the periodic orbit is globally asymptotically stable. To prove this let us introduce the map $\Phi^s$ that associates to any initial datum $x_0$ the value of the corresponding solution at time $s$. Consider a generic initial datum $x_0$ and define the sequence $x_n$ as follows

$$x_{n+1} = \Phi^{2\pi}(x_n) \quad \forall\, n \geq 0. \tag{21}$$

All the limit points of the sequence are fixed point of $\Phi^{2\pi}$. Due to the uniqueness of the periodic orbit, $\Phi^{2\pi}$ has one and only one fixed point which corresponds to the initial datum $\tilde{x}_0$ of the periodic orbit. Notice that since the solutions of (16) are bounded, so is the sequence $(x_n)$. This fact and the uniqueness of the limit point imply by a standard argument that the sequence $(x_n)$ converges to $\tilde{x}_0$, therefore the solution starting from $x_0$ converges to the periodic orbit.

As noted before, the net displacement after one period is proportional, to leading order in the amplitude of the deformations, to the area enclosed by the loops formed in the configuration space. Now we will prove that this area vanishes when either $\Omega \to 0$ or $\Omega \to +\infty$. By some simple inequalities it is possible to show that there exists $G_{\min} > 0$ such that

$$\tilde{G}(\Lambda_1, \Lambda_2) > G_{\min} > 0 \quad \forall \Lambda_1 > 2\alpha. \tag{22}$$

Using this fact we can prove that the velocity field $f$ of eq. (14) is such that

$$\begin{cases} f(\tau, x) < 0, & \text{if } x > \Omega\delta, \\ f(\tau, x) > 0, & \text{if } 2\alpha - \lambda_1 < x < -\Omega\delta, \end{cases} \tag{23}$$

where $\delta := \lambda_2\epsilon/2G_{\min}$. This implies that the loops in the configuration space are contained in the box

$$\Big\{(\Lambda_1, \Lambda_2) : \Lambda_1 \in [\lambda_1 - \Omega\delta, \lambda_1 + \Omega\delta], \\ \Lambda_2 \in [\lambda_2(1-\epsilon), \lambda_2(1+\epsilon)]\Big\}. \tag{24}$$

When $\Omega \to 0$ the area of the box vanishes, and so does the area enclosed by the loops. Now we turn to the case in which $\Omega \to +\infty$. In this case we find the following limit problem

$$\begin{cases} \Lambda_1' = -\tilde{F}(\boldsymbol{\Lambda})\Lambda_2', \\ \Lambda_1(0) = x_0. \end{cases} \tag{25}$$

The solution of (25) has the form

$$\Lambda_1 = \Psi(\Lambda_2), \tag{26}$$

where $\Psi$ is the solution of the following problem:

$$\begin{cases} \Psi'(x) = -F(\Psi(x), x), \\ \Psi(\lambda_2) = \Lambda_1(0). \end{cases} \tag{27}$$

Let us indicate with $\Lambda_1(\tau)$ the solution of (16). When $\Omega \to +\infty$ this solution converges to the solution of (25). In particular the loop enclosed by the trajectory $(\Lambda_1(t), \Lambda_2(t))$ shrinks to the graph of $\Psi$ and therefore the enclosed area vanishes.

Our analysis shows that $\Omega$ plays a fundamental role in determining the behaviour of the system. Obviously, there are different ways of varying $\Omega$. The reference problem we have in mind is the following: the swimmer is given (hence $l$ and $k$ are fixed), and the surrounding fluid is given (hence $\mu$ is fixed), so the only way to vary $\Omega$ is to change the actuation frequency $\omega$. In this case we need to be careful about the results concerning the regime in which $\omega \to +\infty$. These results should be taken with a grain of salt because eqs. (1)–(3), on which all of our analysis is based, hold in the hypothesis that the surrounding fluid is governed by the *steady* Stokes system (rather than by the Navier-Stokes equations). This requires not only that the Reynolds number $Re := VL/\nu$ be vanishing small, but also that the Strouhal number $St := \omega L/V$ be bounded, see *e.g.* [19]. Here $\nu = \mu/\rho$ is the kinematic viscosity of the surrounding fluid ($\nu = 10^6\,(\mathrm{m^2\,s^{-1}})^{-1}$ for water at room temperature), and $V$ and $L$ are the swimming velocity and the size of the swimmer, the typical velocity and length scales for the flow induced by a swimmer in a fluid at rest.

### 3.2 Numerical simulations

In this section we consider the reference problem in which we vary $\omega$ while the other parameters are fixed (see table 1). All numerical simulations are obtained using MATLAB ode45 procedure, which consists of a Runge-Kutta integration scheme with adaptive step size. Figure 2 shows the trajectories in the configuration space: we observe that non-trivial loops are formed. The distance travelled in one period is, to leading order, proportional to the area enclosed by the loop. We thus expect that, if the angular frequency $\omega$ is too small or too large, then the net displacement per period will be small compared to the ones achievable at intermediate frequencies. This is in agreement with the results of the previous section, in which we showed that the area enclosed by the loops vanishes when $\Omega$ goes to zero or to $+\infty$. The swimming velocity of the whole object is the average translational velocity

$$V_0 = \frac{1}{3}(v_1 + v_2 + v_3). \tag{28}$$

Using eqs. (1)–(4) we can show that

$$V_0 = \left(\frac{1}{L_1 + L_2} - \frac{1}{L_2}\right)\frac{f_1}{12\pi\mu} + \left(\frac{1}{L_1 + L_2} - \frac{1}{L_1}\right)\frac{f_3}{12\pi\eta}. \tag{29}$$

Now we can use eqs. (1)–(6) to express $f_1$ and $f_3$ in terms of $L_1$, $L_2$, $\dot{L}_1$, $\dot{L}_2$. If we substitute the resulting expressions in eq. (29) and keep only the leading-order terms in $a/L_j$ we obtain

$$V_0 = \frac{a}{6}\left[\left(\frac{\dot{L}_2 - \dot{L}_1}{L_2 + L_1}\right) + 2\left(\frac{\dot{L}_1}{L_2} - \frac{\dot{L}_2}{L_1}\right) + \frac{\dot{L}_2}{L_2} - \frac{\dot{L}_1}{L_1}\right]. \tag{30}$$

**Table 1.** Values of the parameters used in the numerical simulations. $\mu$ is the dynamic viscosity of water at 25 °C.

| | |
|---|---|
| $l_1$ | $2 \cdot 10^{-4}$ m |
| $l_2$ | $2 \cdot 10^{-4}$ m |
| $a$ | $0.1 \cdot 10^{-4}$ m |
| $\mu$ | $8.9 \cdot 10^{-4}$ Pa s |
| $k$ | $10^{-7}$ Nm$^{-1}$ |

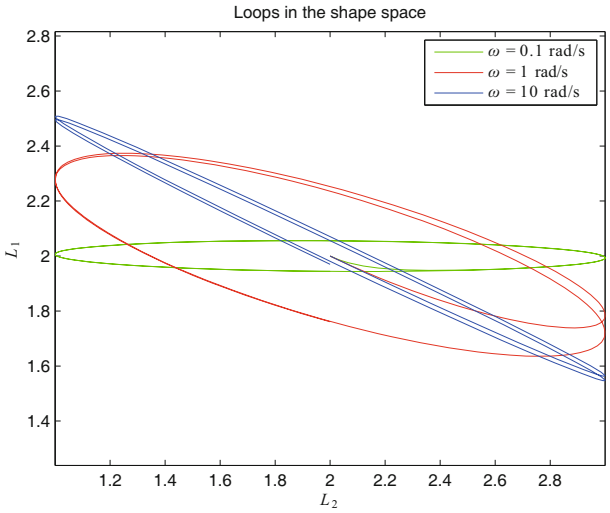


**Fig. 2.** This plot, obtained though numerical integration of (8), shows the curves along which the two shape parameters $L_1$ and $L_2$ evolve. The different colours correspond to different actuation frequencies of the front rod. The unit of length is $10^{-4}$ m. Notice that the area enclosed by the red loop (intermediate actuation frequency) is the largest.

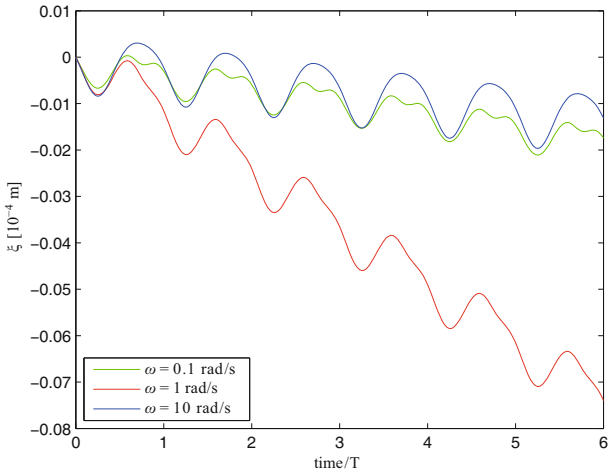


**Fig. 3.** Time evolution of the displacement $\xi$. The graph was obtained through numerical integration of (32). We plot the displacement as a function of the normalized time $t/T$, where $T = 2\pi/\omega$ is the period of the swimmer's stroke. The unit of length is $10^{-4}$ m.

If $\xi_i$ is the position of the $i$-th sphere and $\xi = \frac{1}{3}(\xi_1+\xi_2+\xi_3)$ then obviously

$$\dot{\xi} = V_0. \tag{31}$$

By using this kinematic relation together with eqs. (8) and (30) we obtain a system of ODEs of the form

$$\frac{\mathrm{d}}{\mathrm{d}t}\begin{pmatrix} L_1 \\ \xi \end{pmatrix} = H(t, L_1, \xi), \tag{32}$$

where the components of $H$ are given by the right-hand sides of eqs. (8) and (30), respectively. We integrated this system numerically to investigate the time evolution of $\xi$: the result is shown in fig. 3. There are some interesting facts to point out about this graph. First of all, after 6 periods the swimmer with intermediate actuation frequency has achieved a net displacement which is much larger than those of the other two swimmers, as we expected from the size of the loops in the configuration space. In addition, we notice that the motion is retrograde: the net displacement after one period has a negative sign. Clearly, the motion of these swimmers is rather inefficient, because small net displacements are achieved with large back and forth oscillations.

We conclude with a remark on the formula for $V_0$. When a steady state is reached, both $L_1$ and $L_2$ are periodic functions with period $T$, so the terms $\dot{L}_j/L_j$ average to zero in a full swimming cycle, since they are derivatives of $\log(L_j)$. If we neglect terms which have zero mean over one period we obtain the following formula:

$$V_0 = \frac{a}{6}\left[\left(\frac{\dot{L}_2 - \dot{L}_1}{L_2 + L_1}\right) + 2\left(\frac{\dot{L}_1}{L_2} - \frac{\dot{L}_2}{L_1}\right)\right], \tag{33}$$

which can be used instead of (30) to compute the average velocity in the stationary regime.

## 4 Asymptotic analysis

We assume that solutions of (11) can be expressed in the form

$$\Lambda_1(\tau) = \lambda_1 + \epsilon x_1(\tau) + \epsilon^2 x_2(\tau) + \dots . \tag{34}$$

By expanding the velocity field in (11) in powers of $\epsilon$ we obtain the following equation for the leading-order term:

$$x_1' = -\frac{1}{\Omega} G_0 x_1 - F_0 \lambda_2 \cos(\tau), \tag{35}$$

where $F_0 = F(l_1, l_2)$ and $G_0 = G(l_1, l_2)$, namely,

$$F_0 = \left(\frac{1}{2l_2} - \frac{1}{3a}\right)^{-1}\left(\frac{1}{4l_2} + \frac{1}{4l_1} - \frac{1}{4(l_1+l_2)} - \frac{1}{6a}\right), \tag{36}$$

$$G_0 = \frac{l}{\pi}\left[\left(\frac{1}{3a} - \frac{1}{2l_1}\right) + \left(\frac{1}{2l_2} - \frac{1}{3a}\right)^{-1} \times \left(\frac{1}{4l_2} + \frac{1}{4l_1} - \frac{1}{4(l_1+l_2)} - \frac{1}{6a}\right)^2\right]. \tag{37}$$

Notice that (35) can be seen as the equation of a damped harmonic oscillator with negligible mass and periodic driving force. The solution for the leading-order term is given by

$$x_1(\tau) = -A(\Omega)\lambda_2 \sin(\tau) + B(\Omega)\lambda_2\left[e^{-G_0\tau/\Omega} - \cos(\tau)\right], \tag{38}$$

where

$$A(\Omega) = \frac{\Omega^2}{\Omega^2 + G_0^2} F_0\,, \tag{39}$$

$$B(\Omega) = \frac{\Omega}{\Omega^2 + G_0^2} G_0 F_0\,. \tag{40}$$

We notice from (38) above that the leading-order term has an exponentially decaying term describing a transient, and a term describing a harmonic steady-state response. The relaxation time is $\tau_c = \frac{\Omega}{G_0}$, which is the characteristic relaxation time of the damped harmonic oscillator (35).

In fig. 4 we show a comparison between the loops in the configuration space obtained through numerical integration of (11) and the harmonic steady-state response of the leading-order term (38), in the case $\Omega = G_0$. The result of the numerical integration is plotted with solid lines while the dashed lines show the leading-order approximation. The error due to neglecting higher order terms becomes visible only for large values of $\epsilon$.

Now we would like to compute leading-order expressions of some important physical quantities, namely, displacement per period, average swimming velocity, and mechanical work in one period. First of all we would like to compute the average of $V_0$ over one full swimming cycle in the stationary regime. We can use eq. (33) in which the terms with zero average have been neglected. We consider the case of small deformations

$$L_1 = l_1 + u,$$
$$L_2 = l_2 + v,$$

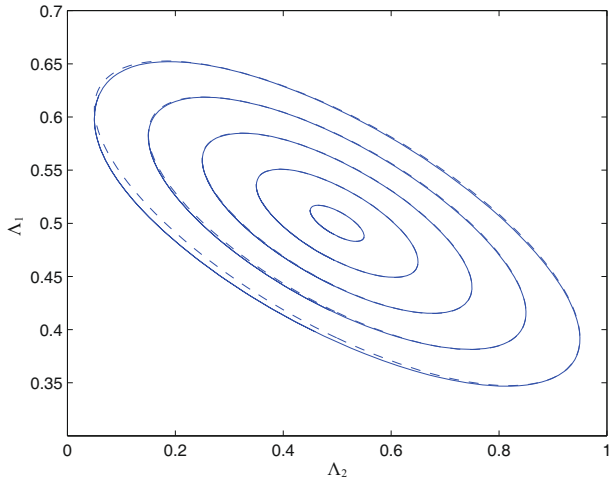


**Fig. 4.** Loops in the shape space: comparison between numerical simulations (solid lines) and leading-order approximation (dashed lines) corresponding to the case $\Omega = G_0$. The biggest loop is obtained for $\epsilon = \epsilon_{\max}$ and the others by decreasing $\epsilon$ in steps of 0.2.

with $u/l_j, v/l_j \ll 1$. Following [5,17], we expand eq. (33) and retain only the leading-order terms in $u/l_j$, $v/l_j$ obtaining

$$V_0 = \frac{a}{6}\left[\frac{\dot{v}-\dot{u}}{l_1+l_2} - \frac{(\dot{v}-\dot{u})(u+v)}{(l_1+l_2)^2} + \frac{2\dot{u}}{l_2} - \frac{2\dot{u}v}{l_2^2} - \frac{2\dot{v}}{l_1} + \frac{2\dot{v}u}{l_1^2}\right]. \tag{41}$$

The terms $\dot{u}$, $\dot{v}$, $\dot{u}u$, $\dot{v}v$, $\dot{u}v + u\dot{v}$ average to zero over one period. So we get the following expression for the average swimming velocity:

$$\overline{V_0} = \frac{1}{T}\int_0^T V_0(s)\mathrm{d}s = \frac{C}{l}\overline{(u\dot{v} - \dot{u}v)}, \tag{42}$$

where

$$C = \frac{al}{6}\left[\frac{1}{l_1^2} + \frac{1}{l_2^2} - \frac{1}{(l_1+l_2)^2}\right].$$

The net displacement per period is $Xl = T\overline{V_0}$. If we non-dimensionalize (42) and set $x = u/l$, $y = v/l$ we obtain

$$X = C\int_0^{2\pi}(xy' - x'y)\mathrm{d}\tau, \tag{43}$$

which expresses the net displacement per period in units of body length. Now we can use (38) to compute a leading-order expression for $X$. The result is the following:

$$X = -2\pi\lambda_2^2 CB(\Omega)\epsilon^2 + O(\epsilon^3). \tag{44}$$

In particular we see that the leading-order term has a negative sign, in agreement with the numerical simulations showing retrograde motion. The negative sign of the displacement is not due to our particular choice of the deformation of the active arm (9). The case of a generic periodic deformation can be studied with the help of a decomposition in Fourier series: the computations are similar to the ones presented here and it is not difficult to see that the sign of $X$ remains negative. So the three-sphere swimmer with passsive elastic arm can only swim with the passive arm ahead. Now we compute the leading-order expression for the mechanical work done by the swimmer in one period. The power expended to drive the active arm is

$$\mathcal{P} = f_3\dot{L}_2. \tag{45}$$

Using eqs. (2), (4), (6), and (7) we find

$$f_3 = \left(\frac{1}{3a} - \frac{1}{2L_2}\right)^{-1}\pi\mu\dot{L}_2 - k(L_1 - l_1)F(\mathbf{L}). \tag{46}$$

Therefore the work done in one period is

$$l^3\mu\omega W = \int_0^T \left(\frac{1}{3a} - \frac{1}{2L_2}\right)^{-1}\pi\mu\dot{L}_2^2 - k(L_1 - l_1)F(\mathbf{L})\dot{L}_2\mathrm{d}t. \tag{47}$$

If we non-dimensionalize the previous equation and use (38), we find a leading-order expression for the dimensionless work in one period:

$$W = \pi\lambda_2^2\left[\pi\left(\frac{1}{3\alpha} - \frac{1}{2\lambda_2}\right)^{-1} + F_0\frac{B(\Omega)}{\Omega}\right]\epsilon^2 + O(\epsilon^3). \tag{48}$$

## 5 Optimal swimming

In this section we study some optimization problems. We take into account the various performance measures considered in [16]. First we study optimization of swimming at fixed geometry. Since the dynamics is entirely controlled by the dimensionless parameter $\Omega$, this means optimizing the different performance measures with respect to $\Omega$. Then we consider optimization with respect to the geometry of the swimmer, namely, we discuss how the different performance measures change when the ratio $\beta = l_1/l_2$ is varied.

### 5.1 Optimization with respect to Ω

In this subsection we study optimization of different performance measures with respect to the parameter $\Omega$. For the computations we use the leading-order expressions obtained in the previous section. Then we compare the results with data obtained from numerical simulations of the full system.

The first performance measure we consider is the net displacement per period. Notice that if we use dimensionless variables then the average velocity over one period coincides (up to a multiplicative constant) with the net displacement per period. Therefore the value of the parameter $\Omega$ optimizing the latter optimizes also the former. For this reason we do not consider the average swimming speed as an independent performance measure. Using eq. (44) it is easy to see that $X$ is optimized when

$\Omega = \Omega_X := G_0$. The corresponding maximal displacement is

$$X^* = -\pi\lambda_2^2 C F_0 \epsilon^2. \tag{49}$$

From eq. (44) we also see that $X$ goes to zero when $\Omega$ goes to either zero or $+\infty$. We discuss below the physical interpretation of this important fact.

To understand what happens in the limit cases, let us consider eq. (35). The term corresponding to the elastic restoring force is $\frac{1}{\Omega} G_0 x_1$. Therefore if $\Omega \to +\infty$ the elastic force becomes negligible with respect to the viscous drag and the passive arm behaves as if it were free. If no elastic force is present, the hydrodynamic forces tend to synchronize the evolution of $\Lambda_1$ and $\Lambda_2$, causing reciprocal shape change and no net motion in view of the scallop theorem. Indeed, if we send $\Omega$ to $+\infty$ in (35) we get the following equation:

$$x_1' = -F_0 \lambda_2 \cos(\tau), \tag{50}$$

with the initial condition $x_1(0) = 0$. The solution is $x_1(\tau) = -F_0\lambda_2 \sin(\tau)$. As a consequence the equation

$$\Lambda_1 = \lambda_1 - F_0(\Lambda_2 - \lambda_2) \tag{51}$$

is satisfied to leading order in $\epsilon$. This implies that the shape change of the swimmer is reciprocal.

If $\Omega$ goes to zero we observe the opposite behaviour: the elastic force dominates and the passive arm behaves as a rigid rod of fixed length $l_1$. Thus, the loops in shape space collapse to a line. In fact, if we multiply eq. (35) by $\Omega$ and send $\Omega$ to 0, we obtain the algebraic equation $x_1 = 0$.

To sum up, in the regime $\Omega \to 0$ the elastic force dominates over viscous drag and makes the passive arm behave as a rigid link. In the regime $\Omega \to +\infty$ the elastic force becomes negligible and the hydrodynamic interactions cause a synchronization of $\Lambda_1$ and $\Lambda_2$. In the two limit cases the swimmer does not achieve net displacement after one period. In the intermediate case $0 < \Omega < +\infty$, the interplay between elastic and hydrodynamic forces causes the formation of loops in the shape space, producing locomotion. The maximal net displacement per period is obtained for $\Omega = G_0$.

The second performance measure we consider is the work per travelled distance

$$\lambda = \frac{W}{|X|}. \tag{52}$$

Using eqs. (44) and (48) we find

$$\lambda = K_1 \Omega + K_2 \frac{1}{\Omega}, \tag{53}$$

where

$$K_1 = \frac{1}{2C}\pi \left(\frac{1}{3\alpha} - \frac{1}{2\lambda_2}\right)^{-1} \frac{1}{G_0 F_0},$$
$$K_2 = \frac{1}{2C}\left[\pi\left(\frac{1}{3\alpha} - \frac{1}{2\lambda_2}\right)^{-1} \frac{G_0}{F_0} + F_0\right].$$

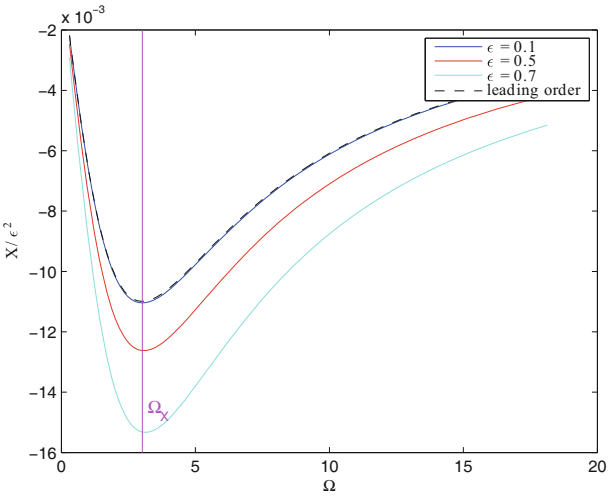


**Fig. 5.** Plot of scaled dimensionless net displacement per period $X/\epsilon^2$ as a function of the parameter $\Omega$. The full lines correspond to numerical simulations of the system with different values of $\epsilon$ while the dashed line shows the leading-order approximation. The vertical line corresponds to $\Omega_X$.

It is easy to see that $\lambda$ is optimized for $\Omega = \Omega_\lambda = \sqrt{K_2/K_1}$ and that the corresponding optimal value is $\lambda^* = 2\sqrt{K_1 K_2}$.

The third performance measure we consider is Lighthill's efficiency. We follow [20] and define

$$\eta := \frac{18\pi\mu a \overline{V_0}^2}{\overline{P}}. \tag{54}$$

If we non-dimensionalize the different quantities we find that $\eta = 9\alpha X^2/W$. By using (44) and (48) we obtain the following leading-order expression

$$\eta = \frac{4\pi\lambda_2^2 C^2 G_0^2 F_0^2 \Omega^2}{(\Omega^2 + G_0^2)(\pi(\frac{1}{3\alpha} - \frac{1}{2\lambda_2})^{-1}(\Omega^2 + G_0^2) + G_0 F_0^2)}\epsilon^2 + O(\epsilon^3). \tag{55}$$

The leading-order term is maximized when $\Omega = \Omega_\eta$, where

$$\Omega_\eta := \left(G_0^4 + \frac{F_0^2 G_0^3}{\pi}\left(\frac{1}{3\alpha} - \frac{1}{2\lambda_2}\right)\right)^{1/4}. \tag{56}$$

We indicate with $\eta^*$ the corresponding maximal efficiency.

It is not difficult to verify that

$$\Omega_X < \Omega_\eta < \Omega_\lambda. \tag{57}$$

The graphs in figs. 5, 6, and 7, obtained from the numerical solutions of the full problem, confirm the reliability of the theoretical predictions about the optimal values of $\Omega$ obtained above on the basis of the leading-order terms.

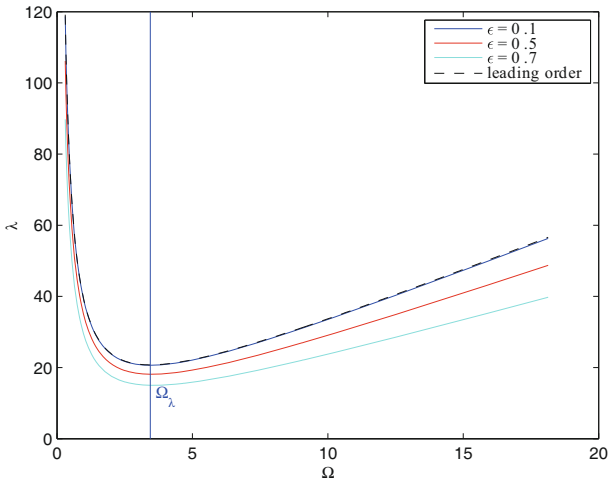


**Fig. 6.** Plot of dimensionless work per travelled distance $\lambda$ as a function of the parameter $\Omega$. The full lines correspond to numerical simulations of the system with different values of $\epsilon$ while the dashed line shows the leading-order approximation. The vertical line corresponds to $\Omega_\lambda$.

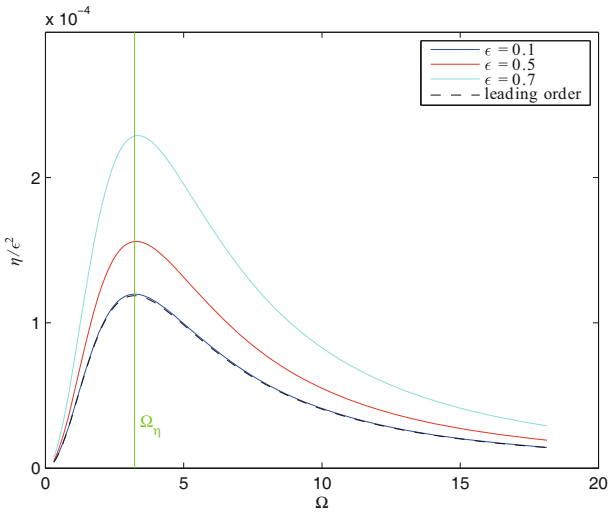


**Fig. 7.** Plot of scaled Lighthill's efficiency as a function of the parameter $\Omega$. The full lines correspond to numerical simulations of the system with different values of $\epsilon$ while the dashed line shows the leading-order approximation. The vertical line corresponds to $\Omega_\eta$.

### 5.2 Optimal geometry

In this section we study optimization of the swimmer's shape. We keep the swimmer's total length $l = l_1 + l_2$ fixed and vary the ratio $\beta := l_1/l_2$. We would like to optimize $X^*$, $\lambda^*$, and $\eta^*$ with respect to $\beta$. First of all we observe that, since $l_1$ and $l_2$ must be greater than $2a$, the acceptable values of $\beta$ are subject to the following restriction:

$$\beta_{\min} := \frac{2a}{l-2a} < \beta < \frac{l-2a}{2a}. \qquad (58)$$

In figs. 8, 9, and 10 we show the plots of the optimal values of the different performance measures as functions of $\beta$.

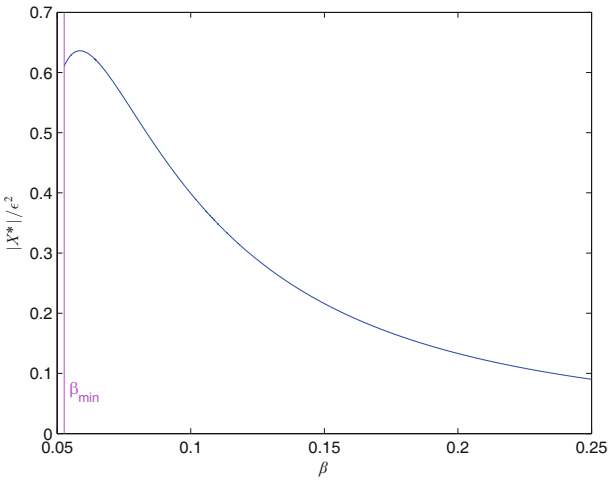


**Fig. 8.** Plot of the scaled optimal net displacement per period $X^*$ as a function of the ratio $\beta = l_1/l_2$. In order to satisfy the natural assumption that $l_1 > 2a$ (no overlapping of spheres 1 and 2 when the spring is at rest), the values of $\beta$ are subject to the restriction $\beta > \beta_{\min}$.

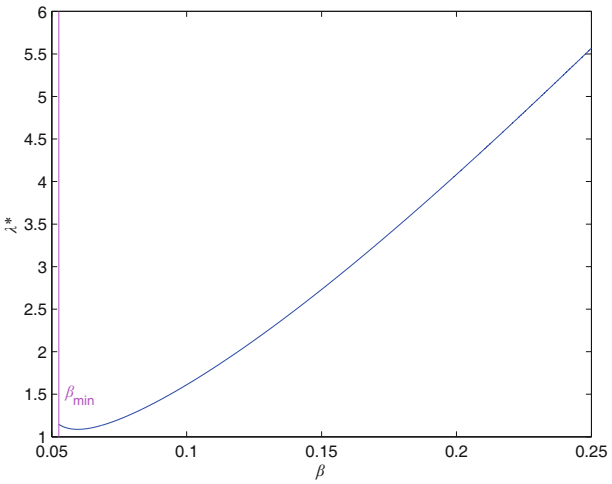


**Fig. 9.** Plot of the optimal work per travelled distance as function of the ratio $\beta = l_1/l_2$. In order to satisfy the natural assumption that $l_1 > 2a$ (no overlapping of spheres 1 and 2 when the spring is at rest), the values of $\beta$ are subject to the restriction $\beta > \beta_{\min}$.

The three different performance measures give different optimal values of $\beta$. These values are strictly greater than $\beta_{\min}$. This analysis has, however, only qualitative value because when $\beta$ is close to $\beta_{\min}$, the hypothesis $a/L_j \ll 1$ on which (1)–(3) and all our subsequent analysis are based no longer holds.

## 6 Conclusions

We analyzed the dynamics of the three-sphere low-Reynolds-number swimmer with an active arm and a passive elastic one. We considered periodic deformations of the active arm with amplitude $\epsilon$ and angular frequency $\omega$. Similarly to the behaviour illustrated in [16], the compe-

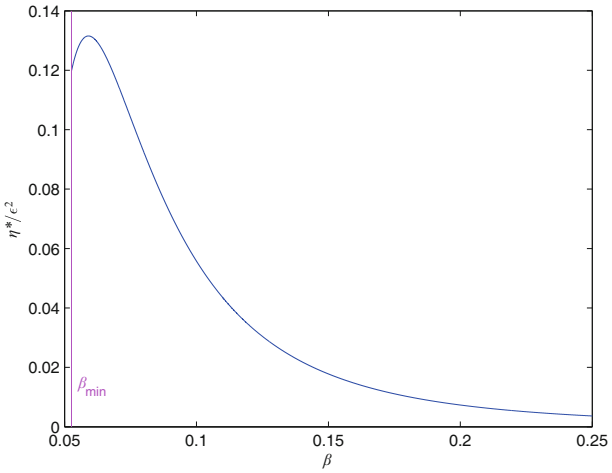


**Fig. 10.** Plot of the scaled optimal Lighthill's efficiency as function of the ratio $\beta = l_1/l_2$. In order to satisfy the natural assumption that $l_1 > 2a$ (no overlapping of spheres 1 and 2 when the spring is at rest), the values of $\beta$ are subject to the restriction $\beta > \beta_{\min}$.

tition between hydrodynamic and elastic forces generates a phase lag in the response of the elastic arm and hence non-reciprocal shape changes and self-propulsion. This implies that a minimal swimmer requires only one device, controlling the length of only one arm, and not two independent ones. However, this is at the expense of losing the possibility of controlling swimming direction. In fact, the three-sphere swimmer with passive elastic arm can move only with the passive arm ahead.

We then addressed some optimal swimming problems. By rewriting the system in dimensionless variables we showed that its behaviour is determined by a parameter $\Omega$ depending on the fluid viscosity, the elastic constant of the spring, the body length of the swimmer and the actuation frequency of the active arm. We considered three different optimality measures: net displacement per period, work per travelled distance, and Lighthill's efficiency. We worked in the framework of small deformations ($\epsilon \ll 1$) and computed leading-order expressions for the different performance measures. By using these leading-order expressions we found three different optimal values of $\Omega$, one for each performance measure. The results of numerical simulations of the full problem show that the optimal values computed using leading-order expressions are a good approximation of the actual optimal values. Finally, we considered the problem of optimizing the geometry of the swimmer. We studied how the optimal values of the different performance measures vary when the ratio between the lengths of the two arms is changed, keeping the total length of the swimmer fixed.

Support by the European Research Council through the ERC Advanced Grant 340685-MicroMotility is gratefully acknowledged. We also thank G. Cicconofri for helpful discussions.

## Appendix A. Periodic perturbations of periodic systems

We collect here some classical results on periodically perturbed dynamical systems that we used in sect. 3.1. We refer to [18] for the proofs. We begin with some definitions. For $t_0 < t_1$ let the matrix function $A : (t_0, t_1) \to \mathbb{R}^{n\times n}$ be continuous. Consider the homogeneous linear system

$$\dot{y} = A(t)y. \tag{A.1}$$

Along with this system we may also consider the following matrix differential equation

$$\dot{Y} = A(t)Y. \tag{A.2}$$

A matrix function $Y : (t_0, t_1) \to \mathbb{R}^{n\times n}$ is a solution of (A.2) if it is $C^1$ and satisfies the equation for every time $t$. A solution of (A.2) is called a *matrix solution* of (A.1). A regular matrix solution is a matrix solution $R(t)$ such that $\det R(t) \neq 0$ for every $t$. A regular matrix solution is called a *fundamental matrix*. We denote with $R(t, s)$ the fundamental matrix that is equal to the $n \times n$ identity matrix at time $s \in (t_0, t_1)$. Now we consider the special case in which $A \in C^0(\mathbb{R}_+, \mathbb{R}^{n\times n})$ and $A$ is periodic with period $T$. In this case the *characteristic multipliers* of system (A.1) are defined as the eigenvalues of the fundamental matrix $R(T, 0)$. Now consider a one parameter family of differential equations

$$\dot{x} = f(t, x) + \epsilon g(t, x, \epsilon), \tag{A.3}$$

where $f$ is a smooth function on $\mathbb{R} \times X$, $X \subseteq \mathbb{R}^n$ an open and connected domain and $g$ is a smooth function on $\mathbb{R} \times X \times I$ where $I$ is an open interval containing $\epsilon = 0$. We assume that $f$ and $g$ are periodic in the variable $t$ with period $T > 0$. The system

$$\dot{x} = f(t, x) \tag{A.4}$$

is called the *unperturbed equation* while (A.3) is the perturbed one. We assume that (A.4) has a periodic solution $p : \mathbb{R} \to X$ with period $T$. This solution will be called the *unperturbed periodic solution*. The variational system of the unperturbed eq. (A.4) with respect to its periodic solution $p$ is the following equation:

$$\dot{y} = D_x f(t, p(t))y, \tag{A.5}$$

where $D_x f$ is the total differential of $f$ with respect to the spatial variables. Now we are ready to give the statement of two important theorems concerning existence and stability of periodic solutions.

Theorem A.1. *If the variational system* (A.5) *does not have non-trivial $T$-periodic solutions or, equivalently,* 1 *is not a characteristic multiplier, then $\epsilon = 0$ has an open neighbourhood $U \subseteq I$ such that for each $\epsilon \in U$ the perturbed system* (A.3) *has one and only one periodic solution $q(t, \epsilon)$ with period $T$ with the properties that $q \in C^1(\mathbb{R} \times U)$ and $q(t, 0) = p(t)$.*

*Proof.* See [18], theorem 6.1.1.

Theorem A.2. *If all the characteristic multipliers of the variational system* (A.5) *are in modulus less than* 1*, then for sufficiently small $|\epsilon|$ the periodic solution $q(t, \epsilon)$ of system* (A.3) *is asymptotically stable.*

*Proof.* See [18], theorem 6.1.3.

## References

1. E.M. Purcell, Am. J. Phys. **45**, 3 (1977).
2. E. Lauga, T.R. Powers, Rep. Prog. Phys. **72**, 096601 (2009).
3. M. Arroyo, L. Heltai, D. Millán, A. DeSimone, Proc. Natl. Acad. Sci. U.S.A. **109**, 17874 (2012).
4. M. Arroyo, A. DeSimone, J. Mech. Phys. Solids **62**, 99 (2014).
5. A. Najafi, R. Golestanian, Phys. Rev. E **69**, 062901 (2004).
6. L.E. Becker, S.A. Koehler, H.A. Stone, J. Fluid Mech. **490**, 15 (2003).
7. J.E. Avron, O. Kenneth, D.H. Oaknin, New J. Phys. **7**, 234 (2005).
8. J.E. Avron, O. Gat, O. Kenneth, Phys. Rev. Lett. **93**, 186001 (2004).
9. D. Tam, A.E. Hosoi, Phys. Rev. Lett. **98**, 068105 (2007).
10. F. Alouges, A. DeSimone, L. Giraldi, M. Zoppello, Int. J. Non-Linear Mech. **56**, 132 (2013).
11. F. Alouges, A. DeSimone, A. Lefebvre, J. Nonlinear Sci. **18**, 277 (2008).
12. F. Alouges, A. DeSimone, A. Lefebvre, Eur. Phys. J. E **28**, 279 (2009).
13. F. Alouges, A. DeSimone, L. Heltai, Math. Models Meth. Appl. Sci. **21**, 361 (2011).
14. F. Alouges, A. DeSimone, L. Heltai, A. Lefebvre, B. Merlet, Discrete Contin. Dyn. Syst. Ser. B **18**, 1189 (2013).
15. A. DeSimone, F. Alouges, L. Heltai, A. Lefebvre, *Natural Locomotion in Fluids and on Surfaces: Swimming, Flying and Sliding*, chapt. "*Computing optimal strokes for low Reynolds number swimmers*" (Springer, 2012) pp. 177–184.
16. E. Passov, Y. Or, Eur. Phys. J. E **35**, 78 (2012).
17. R. Golestanian, A. Ajdari, Phys. Rev. E **77**, 036308 (2008).
18. M. Farkas, *Periodic Motions*, Applied Mathematical Sciences (Springer, New York, 1994).
19. S. Childress, *Mechanics of Swimming and Flying* (Cambridge University Press, 1981).
20. H.A. Stone, A.D.T. Samuel, Phys. Rev. Lett. **77**, 4102 (1996).